Junjie Zhu[1]
Guoqing Hu[2]
Xiangchun Xuan[1]*

[1]Department of Mechanical Engineering, Clemson University, Clemson, South Carolina
[2]LNM Institute of Mechanics, Chinese Academy of Sciences, Beijing, China

Received September 12, 2011
Revised November 1, 2011
Accepted November 6, 2011

Research Article

Electrokinetic particle entry into microchannels

The fundamental understanding of particle electrokinetics in microchannels is relevant to many applications. To date, however, the majority of previous studies have been limited to particle motion within the area of microchannels. This work presents the first experimental and numerical investigation of electrokinetic particle entry into a microchannel. We find that the particle entry motion can be significantly deviated from the fluid streamline by particle dielectrophoresis at the reservoir-microchannel junction. This negative dielectrophoretic motion is induced by the inherent non-uniform electric field at the junction and is insensitive to the microchannel length. It slows down the entering particles and pushes them toward the center of the microchannel. The consequence is the demonstrated particle deflection, focusing, and trapping phenomena at the reservoir-microchannel junction. Such rich phenomena are studied by tuning the AC component of a DC-biased AC electric field. They are also utilized to implement a selective concentration and continuous separation of particles by size inside the entry reservoir.

Keywords:
Electrokinetics / Microfluidics / Dielectrophoresis / Reservoir
DOI 10.1002/elps.201100484

1 Introduction

The fundamental understanding of particle electrokinetics in microchannels is critical to the design and electrical control of microfluidic devices [1–5]. So far there have published many theoretical and experimental papers on electrokinetic particle motion in a variety of microchannels including straight [6–25], curved [26–32], and structured [33–43] ones. However, these studies have all been limited to the particle motion within the area of microchannels. Particles are simply assumed to enter into a microchannel uniformly and can cover the entire microchannel width at the entrance [44]. No attention has been paid to the particle behavior at the reservoir-microchannel junction, which is the indispensable interface between macro and micro worlds in microfluidic devices. As we will demonstrate in this work, the electrokinetic entry motion of particles into a microchannel can be significantly deviated from the fluid streamlines. Particles can actually be aligned, enriched, and sorted at the reservoir-microchannel junction by simply tuning the applied electric field.

In the literature, the very few studies pertinent to electrokinetic transport in microfluidic reservoirs primarily concern the reservoir-induced pressure-driven flow inside the microchannel [45–47]. The pressure gradient can be a consequence of either the finite size of the reservoir [47, 48] or the axial temperature gradients due to the reservoir-based thermal end effects when Joule heating is significant [49, 50]. The resulting pressure-driven flow causes velocity gradients to the plug-like electroosmotic flow and hence increases the sample dispersion [51–53]. It, however, becomes negligible in long microchannels [48, 52]. In contrast, the reservoir effects on electrokinetic particle motion arise from the induced dielectrophoresis (DEP) at the reservoir-microchannel junction due to the inherent non-uniform electric field, which is insensitive to the microchannel length. Such electrokinetic entry motions of particles in microchannels are studied in this work experimentally and numerically.

2 Materials and methods

The microfluidic device was fabricated with poly(dimethylsiloxane) (PDMS) using the standard soft lithography technique. The detailed procedure is given elsewhere [42]. As shown in Fig. 1, the device is composed of a 1-cm-long straight microchannel with two 5-mm-diameter

Correspondence: Professor Guoqing Hu, LNM, Institute of Mechanics, Chinese Academy of Sciences, Beijing 100190, China
E-mail: guoqing.hu@imech.ac.cn

Abbreviation: DEP, dielectrophoresis

*Additional corresponding author: Professor Xiangchun Xuan, E-mail: xcxuan@clemson.edu

Colour online: See the article online to view Figs. 1–4 in colour.

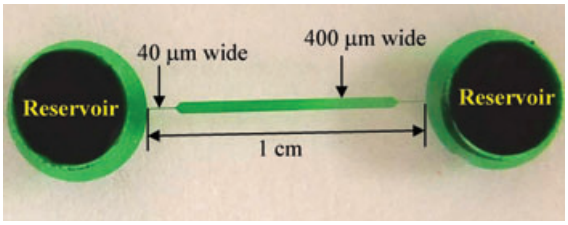

Figure 1. Picture of the microchannel (filled with green food dye for clarity) used in the experiment.

reservoirs at the ends. The channel is 400-μm wide in the middle, which is tapered to 40 μm with a length of 1 mm at each end for the purpose of reducing the applied electric voltage. It is uniformly 25-μm deep. Plain polystyrene particles of 3 μm in diameter (Polysciences, Warrington, PA) were used to study the electrokinetic particle entry into the microchannel. They were also mixed with 1-μm polystyrene particles (Polysciences, Warrington, PA) to demonstrate the size-based particle separation in the reservoir. For both cases, particles were re-suspended in 0.01 × phosphate-buffered saline (PBS) to a final concentration of 10^7–10^8 particles per milliliter. Particle motion was controlled by DC-biased AC electric fields, which were supplied by a function generator (33220A, Agilent Technologies, Santa Clara, CA) in conjunction with a high-voltage amplifier (609E-6, Trek, Medina, NY). The frequency of AC fields was fixed at 1 kHz in all tests. Pressure-driven flow was eliminated by carefully balancing the liquid heights in the two reservoirs prior to measurement. Particle motion was monitored using an inverted microscope (Nikon Eclipse TE2000U, Nikon Instruments, Lewisville, TX), through which videos and images at the constriction region were recorded using a CCD camera (Nikon DS-Qi1Mc, Nikon Instruments, Lewisville, TX).

3 Theory

3.1 Analysis

Due to the significant size mismatch between the macro reservoir and the micro channel, electric field, $\mathbf{E}$, becomes inherently non-uniform at the reservoir-microchannel junction as illustrated in Fig. 2a (the darker the larger magnitude, see Section 3.2 for the computation of $\mathbf{E}$). As such, particles experience a dielectrophoretic force, $\mathbf{F}_{DEP}$, when moving from the reservoir into the microchannel. The time average of $\mathbf{F}_{DEP}$ on an isolated spherical particle under DC and low frequency (<100 kHz) AC electric fields is given by [54]

$$\mathbf{F}_{DEP} = \frac{1}{4}\pi d^3 \varepsilon_f f_{CM} \nabla \mathbf{E}^2 \tag{1}$$

$$f_{CM} = \frac{\sigma_p - \sigma_f}{\sigma_p + 2\sigma_f} \tag{2}$$

where d is the particle diameter, $_f$ is the fluid permittivity, and f_{CM} is the Clausius–Mossotti (CM) factor with σ_p and σ_f being the electric conductivities of the particle and the suspending fluid, respectively. As polystyrene particles [55] and biological cells [56] often appear poorly conducting in DC and low-frequency AC fields, one can have $\sigma_p < \sigma_f$ and hence $f_{CM} < 0$, i.e. negative DEP [57]. Therefore, $\mathbf{F}_{DEP}$ on these particles is directed toward the lower electric field region as indicated by the arrows (length represents the magnitude) in Fig. 2B, where the contour of $|\mathbf{F}_{DEP}|$ (the darker the larger) is also displayed.

The observed particle velocity, $\mathbf{U}_p$, at the reservoir-microchannel junction is the vector addition of the DC electrokinetic velocity (a combination of fluid electroosmosis and particle electrophoresis), $\mathbf{U}_{EK}$, and the AC/DC dielectrophoretic velocity, $\mathbf{U}_{DEP}$ [42, 58]

$$\mathbf{U}_p = \mathbf{U}_{EK} + \mathbf{U}_{DEP} = \mu_{EK}\mathbf{E}_{DC} + \mu_{DEP}\nabla\mathbf{E}^2 \tag{3}$$

$$\mu_{EK} = f_g \varepsilon_f (\zeta_p - \zeta_w)/\mu_f \ ; \text{ and } \ \mu_{DEP} = \varepsilon_f d^2 f_{CM}/12\mu_f \tag{4}$$

where μ_{EK} is the electrokinetic mobility of particles, $\mathbf{E}_{DC}$ is the DC component of the applied electric field, μ_{DEP} is the dielectrophoretic mobility of particles, f_g is the factor accounting for the wall effects on particle motion that is close to 1 for the particles used in our experiments [59], ζ_p is the particle zeta potential, ζ_w is the wall zeta potential, and μ_f is the fluid viscosity. Note that we have neglected particle inertial, Brownian, and gravitational motions in Eq. (3), which is reasonable in typical electrokinetic microfluidic devices [3]. In our experiment, ζ_p is significantly different from ζ_w in magnitude. According to Ermolina and Morgan [54] and Kirby et al. [60], we estimate that the average zeta potentials of the polystyrene particles and the PDMS/glass channel walls are about −40 mV and −80 mV, respectively, in the 1 mM buffer solution. These two values yield an electrokinetic mobility that seems to be consistent with the measured one, $\mu_{EK} = 2.7 \times 10^{-8}$ (m^2/V·s). The measurement method will be presented in the next section.

Similar to a constriction microchannel [42, 58], there exist two sources of electric field non-uniformities at the reservoir-microchannel junction: one is due to the reduction in cross-sectional area from reservoir to microchannel that gives rise to electric field gradients primarily parallel to the streamlines, and the other is due to the discrepancy in path length for electric current around the corners of the junction that causes electric field gradients mainly normal to the streamlines; see $\mathbf{F}_{DEP}$ in Fig. 2b and the electric field lines (equivalent to streamlines [61]) in Fig. 2c. Therefore, particle velocity, $\mathbf{U}_p$, can be conveniently expressed in terms of the traditional streamline coordinates as illustrated by the particle velocity analysis in Fig. 2C,

$$\begin{aligned}\mathbf{U}_p &= (U_{EK} + U_{DEP,s})\hat{\mathbf{s}} + U_{DEP,n}\hat{\mathbf{n}} \\ &= \left(\mu_{EK} E_{DC} + \mu_{DEP}\frac{\partial E^2}{\partial s}\right)\hat{\mathbf{s}} + \left(2\mu_{DEP}\frac{E^2}{\Re}\right)\hat{\mathbf{n}}\end{aligned} \tag{5}$$

where U_{EK} is the magnitude of the streamwise electrokinetic velocity, $U_{DEP,s}$ is the magnitude of the streamwise dielectrophoretic particle velocity, $\hat{\mathbf{s}}$ is the unit vector of the

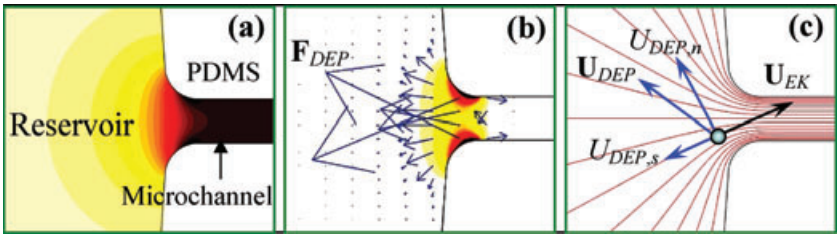

Figure 2. (a) Contour (the darker the larger) of electric field magnitude, $|\mathbf{E}|$, (b) contour and direction of the induced dielectrophoretic force, $\mathbf{F}_{DEP}$, and (c) particle velocity analysis (background shows the streamlines in the absence of the particle) at the reservoir-microchannel junction.

coordinate s along the streamlines, $U_{DEP,n}$ is the magnitude of the cross-stream dielectrophoretic particle velocity, $\hat{\mathbf{n}}$ is the unit vector of the coordinate normal to the streamlines, and $\Re$ is the local radius of curvature of the streamline. Note that only the DC field component, E_{DC}, drives electrokinetic particle motion while particle DEP is induced by the gradient of the total electric field squared, $E^2 = E_{DC}^2 + E_{AC}^2$. This feature greatly facilitates the electric control of particle transport in microfluidic devices as demonstrated previously [29, 31, 39, 42, 58].

For particles experiencing negative DEP, $\mathbf{U}_{DEP,n}$ points toward the centerline of the microchannel as illustrated in Fig. 2C, indicating a particle focusing effect. The effectiveness of this focusing is determined by the ratio of the particle velocities perpendicular and parallel to the streamline, i.e.

$$\left|\frac{U_{DEP,n}}{U_{EK}+U_{DEP,s}}\right| = \frac{2(1+\alpha^2)\frac{E_{DC}}{\Re}}{\frac{\mu_{EK}}{-\mu_{DEP}} - 2(1+\alpha^2)\frac{\partial E_{DC}}{\partial s}} \tag{6}$$

where $\alpha = E_{AC}/E_{DC}$ is the root-mean-square (RMS) AC to DC field ratio, equivalent to the ratio of RMS AC to DC voltage. Note that $\mu_{DEP} < 0$ for negative particle DEP and so $\mu_{EK}/(-\mu_{DEP}) > 0$. Apparently the particle focusing effectiveness increases with the rise of α and E_{DC}. Such DEP-based focusing can also be enhanced by reducing the microchannel dimension [reflected by $\partial E_{DC}/\partial s$ in Eq. (6)] and/or the corner radius of the reservoir-microchannel junction (reflected by $\Re$). Moreover, it favors particles with a small mobility ratio, $\mu_{EK}/(-\mu_{DEP})$, which is expressed as

$$\frac{\mu_{EK}}{-\mu_{DEP}} = \frac{12 f_g(\zeta_p - \zeta_w)}{d^2}\frac{\sigma_p + 2\sigma_f}{\sigma_p - \sigma_f} \tag{7}$$

For instance, larger particles can be more easily focused at the reservoir-microchannel junction than smaller ones.

As to $U_{DEP,s}$, it is against U_{EK} for negative DEP and thus slows down the entering particles at the reservoir-microchannel junction, see Fig. 2C. Moreover, since $U_{DEP,s}$ is a second-order function of the total electric field while U_{EK} is only linearly proportional to the DC field component (see Eq. (5)), one can expect $U_{DEP,s}$ to counter-balance U_{EK} when E increases or E_{DC} decreases. Then, the streamwise particle velocity vanishes and the particle can be stagnated in front of the reservoir-microchannel junction by the locally induced negative DEP,

$$\mu_{EK}E_{DC} + \mu_{DEP}\frac{\partial E^2}{\partial s} \le 0 \quad \text{or} \quad \frac{\mu_{EK}}{-\mu_{DEP}} \le 2(1+\alpha^2)\frac{\partial E_{DC}}{\partial s} \tag{8}$$

The required value of E_{DC} (or equivalently E if α is fixed) and α for trapping particles increases with the increasing particle mobility ratio, $\mu_{EK}/(-\mu_{DEP})$, which, as read from Eq. (7), is a function of the intrinsic properties of particles including size (d), charge (ζ_p), conductivity (σ_p), and permittivity (ε_p). This indicates that we can potentially trap and concentrate one type of particles (e.g. with a larger d) in the entry reservoir while sweeping the other type (e.g. with a smaller d) to the exit reservoir based on any one or combination of these intrinsic particle properties. It is, however, acknowledged that the principle behind the particle focusing, trapping, and separation phenomena at the reservoir-microchannel junction is similar to that inside a constriction microchannel reported in our previous studies [42, 58]. However, the current work is unique as the particle manipulation is completed inside the entry reservoir of the microchannel without the need of any in-channel micro-structures (such as the constriction in refs. 42 and 58, and various other micro-insulators [33, 35, 38, 39, 43]).

3.2 Modeling

We developed a 2D numerical model in COMSOL (Burlington, MA) to simulate the electrokinetic entry motion of particles in microchannels. This model neglects the effects from the top and bottom channel walls on particle transport, which has been proved reasonable in our previous studies [27–29, 35, 42, 58]. It also neglects the perturbations of particles to the flow and electric fields, and instead employs a correction factor, c, to account for the effects of particle size on dielectrophoretic velocity. Hence, the particle velocity in Eq. (3) is rewritten as

$$\mathbf{U}_p = \mu_{EK}\mathbf{E}_{DC} + c\mu_{DEP}(1+\alpha^2)\nabla\mathbf{E}_{DC}^2 \tag{9}$$

This velocity is used as an input of the particle tracing function in COMSOL to compute the particle trajectory. The computational domain comprises the entire microchannel and the two reservoirs. The DC electric field distribution, $\mathbf{E}_{DC} = -\nabla\phi_{DC}$, is obtained by solving the Laplace equation $\nabla^2\phi_{DC} = 0$ with ϕ_{DC} being the DC electric potential. The electrode in each reservoir is simulated by a 0.5-mm-diameter concentric circle, upon which an electric potential is imposed. Specifically, the experimentally applied DC voltage is imposed to the electrode in the entry reservoir. The electrode in the exit reservoir is grounded. All channel walls are assumed electrically non-conducting.

To compute the particle velocity using Eq. (9), the electrokinetic mobility, μ_{EK}, was determined by tracking the motions of individual particles in the main body of the microchannel (where DEP is negligible) under a small DC field. Within the range of experimental errors, we obtained an approximately identical electrokinetic mobility for 1-μm and 3-μm particles, $\mu_{EK} = 2.7 \times 10^{-8}$ (m^2/V·s). It is noted that previous theoretical studies predict a dependence of μ_{EK} on particle size in confined channels [59]. This dependence was, however, found very weak for the two particles used in our experiments. The dielectrophoretic mobility, μ_{DEP}, was calculated from Eq. (4) with the typical dynamic viscosity, $\mu = 1.0 \times 10^{-3}$ kg/(m·s) and permittivity $\varepsilon_f = 6.9 \times 10^{-10}$ C/(v·m) for pure water at 20°C. The electric conductivity of polystyrene particles was estimated using $\sigma_p = 4K_s/d$ with $K_s = 1$ nS being the surface conductance recommended by Ermolina and Morgan [54]. As the electric conductivity of the suspending fluid (i.e. 0.01× PBS) measured 200 μS/cm, the CM factors for 1-μm and 3-μm particles were calculated as −0.36 and −0.45, respectively. The correction factors for these two particles were set to 0.9 and 0.6, both of which are consistent with previous studies [27–29, 35, 42, 58]. A total of 21 evenly distributed points along the electrode surface (i.e. the concentric circle in the model) in the entry reservoir were selected as the initial positions of the uniformly distributed particles therein.

4 Results and discussion

4.1 Particle deflection, focusing, and trapping at the reservoir-microchannel junction

Figure 3 shows the experimentally obtained snapshot (top row) and superimposed (middle row) images of 3-μm particles when they move from the reservoir into the microchannel. The applied DC voltage between the two electrodes in the reservoirs is fixed at 50 V, yielding an average DC electric field of 50 V/cm over the channel. The RMS AC voltage is varied to examine how the AC to DC voltage ratio affects the electrokinetic particle entry into the microchannel. The measured electric current remains constant during the entire experiment indicating negligible Joule heating effects [53]. With no application of the AC voltage, i.e. the AC to DC field ratio is $\alpha = 0$, particles undertake a pure DC electrokinetic motion and move into the microchannel uniformly. As seen in Fig. 3a, particles can cover nearly the entire width of the microchannel, indicating a very weak influence of the induced negative DEP at the reservoir-microchannel junction. However, when an AC voltage with a gradually increasing magnitude is combined to the DC voltage, particles are observed to move away from the corners of the junction and are depleted from the near-wall regions. This is demonstrated in Fig. 3b, where the AC voltage is 200 V or the AC to DC field ratio is $\alpha = 4$. As the AC voltage is increased to 450 V (i.e. $\alpha = 9$), particles are apparently squeezed to a stream flowing in the channel center region as shown in Fig. 3c. With the further increase of α to 13, i.e. the RMS AC voltage is 650 V, all particles travel in a single file along the channel centerline. This is evidenced by the snapshot image in Fig. 3d (top), which can potentially be used to align particles for applications like micro flow cytometry. Such an increasing trend in particle focusing with α is consistent with our analysis in Section 3.1, see Eq. (6).

When the AC voltage is increased to 950 V (i.e. $\alpha = 19$), particles get trapped inside the reservoir right before entering the microchannel. They first form pearl chains, which then extend and turn into clusters as more particles are captured, see Fig. 3e. This phenomenon may be used with potential to filter unwanted particles from the suspending medium for applications such as water purification, or to concentrate rare particles to a detectable level for applications such as biosensing. The simulated particle trajectories at the experimental conditions are shown in the bottom row of Fig. 3, which agree reasonably well with the observations in all cases. This agreement verifies the analysis that we make in Section 3.1 and validates the numerical model we develop in Section 3.2. It is important to note that the above-presented particle deflection, focusing, and trapping phenomena at the reservoir-microchannel junction under DC-biased AC electric fields (i.e. $\alpha > 0$) can also take place when a pure DC voltage (i.e. $\alpha = 0$) is applied and increased. However, the magnitude of the pure DC voltage should be much larger than the total of the DC and AC voltages in the former as read from Eqs. (6) and (8). This is because a larger DC field generates a larger electrokinetic motion, which DEP (though increased, too) has to overcome to achieve particle immobilization. In contrast, the increase of AC field enhances DEP without increasing electrokinetic motion. In addition, we used a dilute concentration of particles in our experiments, such that the particle–particle interactions are weak unless the particles get trapped. This justifies the numerical model where only single particles are considered. However, we believe the particle concentration should affect the demonstrated focusing and trapping phenomena, which will be studied in the future.

4.2 Particle concentration and separation at the reservoir-microchannel junction

We show in this section that the demonstrated particle trapping phenomenon at the reservoir-microchannel junction can be utilized to implement a selective concentration and separation of particles by size inside the reservoir. To do this, we mixed 1-μm particles into the 3-μm particle solution used in the above experiment. As these two particles have approximately the same electrokinetic mobility, 3-μm particles possess a smaller mobility ratio, $\mu_{EK}/(-\mu_{DEP})$, than 1-μm particles as indicated by Eq. (7). Therefore, we should be able to selectively concentrate 3-μm particles in the entry reservoir under an appropriate DC-biased AC electric field, at which 1-μm particles are too small to be trapped by the induced negative DEP and thus swept to the exit reservoir.

Figure 4 shows the results from this experiment, where the experimental images (left panel for snapshot and middle

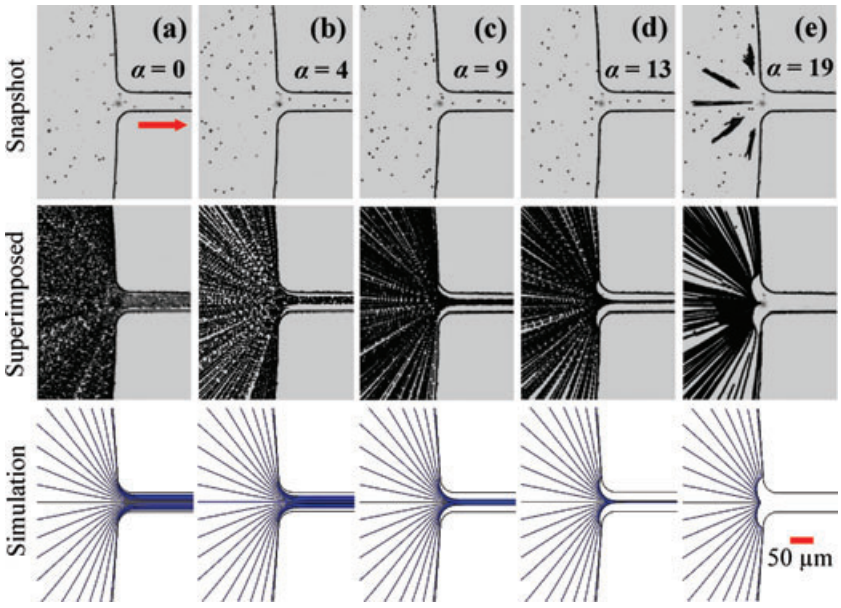

Figure 3. Comparison of experimentally obtained images (snapshot in the top row and superimposed in the middle row) and numerically predicted trajectories (bottom row) of 3 μm particles at the reservoir-microchannel junction under various DC-biased AC electric fields. The applied DC voltage is fixed at 50 V while the RMS AC voltage is varied from (a) 0 V ($\alpha = 0$) to (b) 200 V ($\alpha = 4$), (c) 450 V ($\alpha = 9$), (d) 650 V ($\alpha = 13$), and (e) 950 V ($\alpha = 19$) where α is the AC to DC voltage ratio. The block arrow indicates the flow direction.

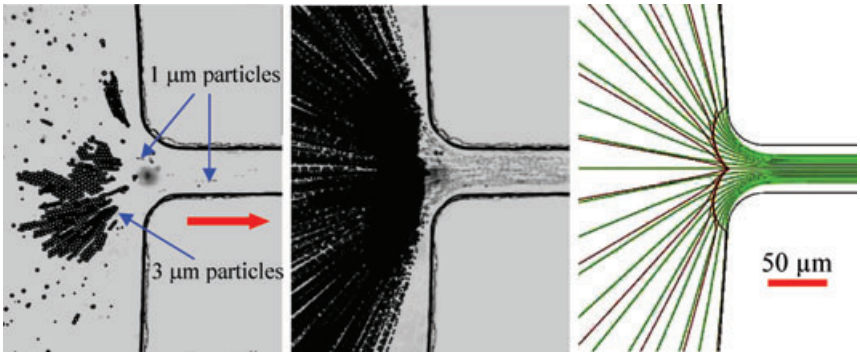

Figure 4. Selective concentration and separation of 3 μm particles from 1 μm particles at the reservoir-microchannel junction under the applied voltage of 50 V DC/950 V AC ($\alpha = 19$). The left, middle, and right panels display the snapshot image, superimposed image, and numerical prediction of the process, respectively. The block arrow indicates the flow direction.

panel for superimposed) are compared with the numerical prediction (right panel). It is found that with the application of 50 V DC/950 V AC, 3-μm particles are accumulated in front of the microchannel entrance, which is consistent with what we observed in Fig. 3e. In contrast, 1-μm particles can pass through the microchannel though in a confined stream along the centerline (see the superimposed image). Moreover, the trapped 3-μm particles seem to have little impact on the electrokinetic entry motion of 1-μm particles, as evidenced in the attached video clip (see the Supporting Information). This indicates an excellent purity for the demonstrated particle separation. The observed concentration and separation processes of the two sizes of particles are both reasonably predicted in our numerical model as illustrated in Fig. 4 (see the middle and right plots). Principally any two types of particles differing in the mobility ratio, $\mu_{EK}/(-\mu_{DEP})$, can be separated inside the reservoir using the same method. However, the mutual influences of the two particles on their respective electrokinetic entry motions are anticipated to increase quickly with the decreased discrepancy in $\mu_{EK}/(-\mu_{DEP})$, which should reduce the separation performance. In addition, the concentration of either of the two particles is believed to affect the trapping and separation processes, which will be studied in the future.

5 Concluding remarks

We have studied the electrokinetic entry motion of particles in a microchannel under DC-biased AC electric fields using a combined experimental and numerical method. By tuning the AC field component while maintaining the DC component, we find that 3-μm particles can be deflected, aligned and trapped at the reservoir-microchannel junction. These phenomena arise from the induced dielectrophoretic particle motion as a result of the inherent non-uniform electric field at the junction. We have also implemented a selective concentration and continuous separation of 3-μm particles from 1-μm particles inside the reservoir by the use of the particle trapping phenomenon at the reservoir-microchannel junction. The observed-rich behaviors of electrokinetic particle entry into the microchannel are all reasonably predicted by our numerical model. The diverse particle manipulations at the reservoir-microchannel junction as demonstrated here are envisioned to find direct near-term applications in a wide range of technological solutions such as flow cytometry (via focusing), filtration (via trapping), biosensing (via concentration), and continuous-flow sorting (via separation).

This work was supported by NSF under Grant No. CBET-0853873 and by Clemson University through a start-up package to X. Xuan. The support from the National 973 Project (Grant No 2011CB707604), NSFC (Grant No 50890182), and Knowledge Innovation Program of CAS (KJCX2-YW-H18) to G. Hu is also gratefully appreciated.

The authors have declared no conflict of interest.

6 References

[1] Bousse, L., Cohen, C., Nikiforov, T., Chow, A., Kopf-Sill, A. R., Dubrow, R., Parce, J. W., *Annu. Rev. Biophys. Biomolecul. Struct.* 2000, *29*, 155–181.

[2] Wong, P. K., Wang, T., Deval, J. H., Ho, C. M., *IEEE/ASME Trans. Mechatron.* 2004, *9*, 366–376.

[3] Li, D., *Electrokinetics in Microfluidics*, Academic Press, London 2004.

[4] Kang, Y., Li, D., *Microfluid. Nanofluid.* 2009, *6*, 431–460.

[5] Regtmeier, J., Eichhorn, R., Viefhues, M., Bogunovic, L., Anselmetti, D., *Electrophoresis* 2011, *32*, 2253–2273.

[6] Keh, H. J., Anderson, J. L., *J. Fluid Mech.* 1985, *153*, 417–439.

[7] Keh, H. J., Lien, L. C., *J. Fluid Mech.* 1991, *224*, 305–333.

[8] Keh, H. J., Chiou, J. Y., *AICHE J.* 1996, *42*, 1397–1406.

[9] Shugai, A. A., Carnie, S. L., *J. Colloid Interf. Sci.* 1999, *213*, 298–315.

[10] Ye, C., Sinton, D., Erickson, D., Li, D., *Langmuir* 2002, *18*, 9095–9101.

[11] Yariv, E., Brenner, H., *Phys. Fluid* 2002, *14*, 3354–3357.

[12] Yariv, E., Brenner, H., *SIAM J. Appl. Math.* 2003, *64*, 423–441.

[13] Hsu, J. P., Ku, M. H., Kao, C. Y., *J. Colloid Interf. Sci.* 2004, *276*, 248–254.

[14] Ye, C., Xuan, X., Li, D., *Microfluid. Nanofluid.* 2005, *1*, 234–241.

[15] Xuan, X., Ye, C., Li, D., *J. Colloid Interf. Sci.* 2005, *289*, 286–290.

[16] Davison, S. M., Sharp, K. V., *J. Colloid Interf. Sci.* 2006, *303*, 288–297.

[17] Liu, H., Qian, S., Bau, H. H., *Biophys. J.* 2007, *92*, 1164–1177.

[18] Unni, H. N., Keh, H. J., Yang, C., *Electrophoresis* 2007, *28*, 658–664.

[19] Hsu, J. P., Chen, Z. S., *Langmuir* 2007, *23*, 6198–6204.

[20] Qian, S., Joo, S. W., Hou, W. S., Zhao, X. X., *Langmuir* 2008, *24*, 5332–5340.

[21] Wang, L. J., Keh, H. J., *J. Phys. Chem. C* 2009, *113*, 12790–12798.

[22] Ai, Y., Beskok, A., Gauthier, D. T., Joo, S. W., Qian, S., *Biomicrofluidics* 2009, *3*, 044110.

[23] Li, D., Daghighi, Y., *J. Colloid Interf. Sci.* 2010, *342*, 638–642.

[24] Liang, L., Qian, S., Xuan, X., *J. Colloid Interf. Sci.* 2010, *350*, 377–379.

[25] Liang, L., Ai, Y., Zhu, J., Qian, S., Xuan, X., *J. Colloid Interf. Sci.* 2010, *347*, 142–146.

[26] Davison, S. M., Sharp, K. V., *Microfluid. Nanofluid.* 2008, *4*, 409–418.

[27] Zhu, J., Tzeng, T. R., Hu, G., Xuan, X., *Microfluid. Nanofluid.* 2009, *7*, 751–756.

[28] Zhu, J., Xuan, X., *J. Colloid Interf. Sci.* 2009, *340*, 285–290.

[29] Church, C., Zhu, J., Wang, G., Tzeng, T. J., Xuan, X., *Biomicrofluidics* 2009, *3*, 044109.

[30] Ai, Y., Park, S., Zhu, J., Xuan, X., Beskok, A., Qian, S., *Langmuir* 2010, *26*, 2937–2944.

[31] Church, C., Zhu, J., Nieto, J., Keten, G., Ibarra, E., Xuan, X., *J. Micromech. Microeng.* 2010, *20*, 065011.

[32] Zhu, J., Tzeng, T. R., Xuan, X., *Electrophoresis* 2010, *31*, 1382–1388.

[33] Lapizco-Encinas, B. H., Simmons, B. A., Cummings, E. B., Fintschenko, Y., *Electrophoresis* 2004, *25*, 1695–1704.

[34] Xuan, X., Xu, B., Li, D., *Anal. Chem.* 2005, *77*, 4323–4328.

[35] Kang, K. H., Xuan, X., Kang, Y., Li, D., *J. Appl. Phys.* 2006, *99*, 064702.

[36] Xuan, X., Raghibizadeh, R., Li, D., *J. Colloid Interf. Sci.* 2006, *296*, 743–748.

[37] Qian, S. Z., Wang, A. H., Afonien, J. K., *J. Colloid Interf. Sci.* 2006, *303*, 579–592.

[38] Pysher, M. D., Hayes, M. A., *Anal. Chem.* 2007, *79*, 4552–4557.

[39] Hawkins, B. G., Smith, A. E., Syed, Y. A., Kirby, B. J., *Anal. Chem.* 2007, *79*, 7291–7300.

[40] Yariv, E., Dorfman, K. D., *Phys. Fluid.* 2007, *19*, 037101.

[41] Ai, Y., Joo, S. W., Jiang, Y., Xuan, X., Qian, S., *Electrophoresis* 2009, *30*, 2499–2506.

[42] Zhu, J., Xuan, X., *Electrophoresis* 2009, *30*, 2668–2675.

[43] Ai, Y., Qian, S., Liu, S., Joo, S. W., *Biomicrofluidics* 2010, *4*, 013201.

[44] Kang, Y., Li, D., *Microfluid. Nanofluid.* 2009, *6*, 431–460.

[45] Yang, R. J., Fu, L. M., Hwang, C. C., *J. Colloid Interf. Sci.* 2001, *244*, 173–179.

[46] Xuan, X., Sinton, D., Li, D., *Int. J. Heat Mass Transfer* 2004, *47*, 3145–3157

[47] Yan, D., Yang, C., Huang, X., *Microfluid. Nanofluid.* 2007, *3*, 333–340.

[48] Yang, R. J., Tseng, T. I., Chang, C. C., *J. Micromech. Microeng.* 2005, *15*, 254–262.

[49] Xuan, X., Xu, B., Sinton, D., Li, D., *Lap. Chip.* 2004, *4*, 230–236.

[50] Tang, G., Yan, D., Yang, C., Gong, H., Chai, C., Lam, Y., *Electrophoresis* 2006, *27*, 628–639.

[51] Tang, G., Yang, C, Chai, C., Gong, H., *Anal. Chim. Acta* 2004, *507*, 27–37.

[52] Xuan, X., Li, D., *J. Chroma. A* 2005, *1064*, 227–237.

[53] Xuan, X., *Electrophoresis* 2008, *29*, 33–43.

[54] Morgan, H., Green, N. G., *AC Electrokinetics: Colloids and Nanoparticles*, Research Studies Press, Hertfordshire, UK 2002.

[55] Ermolina, I., Morgan, H., *J. Colloid. Interf. Sci.* 2005, *285*, 419–428.

[56] Pethig, R., Markx, G. H., *Trends Biotechnol.* 1997, *15*, 426–432.

[57] Voldman, J., *Annu. Rev. Biomed. Eng.* 2006, *8*, 425–454.

[58] Church, C., Zhu, J., Huang, G., Tzeng, T., Xuan, X., *Biomicrofluidics* 2010, *4*, 044101.

[59] Anderson, J. L., *Annu. Rev. Fluid Mech.* 1989, *21*, 61–99.

[60] Kirby, B. J., Hasselbrink, E. F. Jr., *Electrophoresis* 2004, *25*, 203–213.

[61] Cummings, E. B., Griffiths, S. K., Nilson, R. H., Paul, P. H., *Anal. Chem.* 2000, *72*, 2526–2532.

